Numerical study of shear stress distribution at sand ripple surface in wind tunnel flow

Nitsan Bar [a], Tov Elperin [a], Itzhak Katra [b], Hezi Yizhaq [c,d,*]

[a] Department of Mechanical Engineering, The Pearlstone Center for Aeronautical Engineering Studies, Ben-Gurion University of the Negev, P. O. B. 653, 8410501, Israel
[b] Department of Geography and Environmental Development, Ben-Gurion University of the Negev, P. O. B. 653, 8410501, Israel
[c] Swiss Institutes for Dryland Environmental and Energy Research, BIDR, Ben-Gurion University of the Negev, Midreshet Ben-Gurion, Israel
[d] The Dead Sea and Arava Science Center, Tamar Regional Council, Israel

ARTICLE INFO

ABSTRACT

The mechanism responsible for the formation and sustainability of sand ripples sheared by a uniform air flow is not well understood, despite the significant attention that has been given to it ever since the pioneering studies of Bagnold (1941). In this study we explore ANSYS Fluent simulations of fine-scale turbulent flow structure in the vicinity of 2D sand ripples with particular emphasis on shear stress distribution at the sand bed. The flow parameters in the simulations were pertinent to the wind tunnel experiments for studying sand ripples formation. The simulations show that the shear stress at the crest is about 2.5 times larger than the shear stress at the trough and that in most of the simulations a separation bubble has been developed at the lee slope. In contrast to wind tunnel experiments the simulations show that ripples will be flattened at wind speed of 9 m/s as shear stress at the ripples surface exceeds the fluid threshold. This discrepancy between the calculations and real wind tunnel measurements are due to the important role of the saltation layer on the decrease of the shear stress at the surface. Without this effect ripples cannot grow higher and will be diminished at quite moderate winds.

© 2016 Elsevier B.V. All rights reserved.

1. Introduction

One of the open questions in aeolian geomorphology concerns the formation of aeolian sand ripples in the desert or in sand beaches. Although this problem has been investigated by many researchers in the past (e.g. Bagnold, 1941; Sharp, 1963; Anderson, 1987; Yizhaq et al., 2004; Durán et al., 2014; Rasmussen et al., 2015) there are still a number of unresolved or insufficiently explored aspects of sand ripples formation: (i) combined effect of saltation, reptation, suspension and splashing on ripple formation (see e.g. Manukyan and Progozhin (2009) and Kok et al. (2012); for discussions); (ii) effect of electric forces in sand ripple formation (see e.g. Kok (2008)); (iii) influence of grain size distribution on the formation of ripples (Anderson and Bunas, 1993); (iv) mechanism for ripples merging (see Prigozhin (1999)); (v) effect of temperature gradient in the vicinity of the sand bed on ripple formation; (vi) mechanism that limits sand ripples growth;

(vii) mechanism which determines the ripples wavelength (Durán et al., 2014).

Clearly, detachment of sand particles depends strongly on their diameter, adhesion forces, soil wetness, flow parameters such as pressure, temperature and velocity and fluid parameters such as viscosity and molecular structure. One simple characterization of the flow and the fluid parameters is the shear velocity at the surface u_* defined as $u_* = \sqrt{\tau/\rho}$, where τ is the local shear stress and ρ is the local fluid density. According to Shao and Lu (2000) the critical threshold shear velocity for the initiation of motion for static grains is given by the following relation:

$$u_{*t} = \sqrt{0.0123\left(sgd + \frac{3.0 \cdot 10^{-4}}{\rho \cdot d}\right)}, \tag{1}$$

where s is the ratio between the sediment density and the fluid density, g is the acceleration due to gravity and d is the grain diameter. Similar equation that is still used in the literature was suggested by Bagnold (1941):

$$u_{*t} = A\sqrt{\frac{\rho_s - \rho}{\rho}gd}, \tag{2}$$

* Corresponding author at: Swiss Institutes for Dryland Environmental and Energy Research, BIDR, Ben-Gurion University of the Negev, Midreshet Ben-Gurion, Israel.
    E-mail address: hezi.yizhaq1@gmail.com (H. Yizhaq).

where ρ_s is the grain density and ρ is the air density, and A is a coefficient ($A \approx 0.1$) that depends on the grain Reynolds number (Wiggs, 1997). It must be noted that Eq. (2) does not take into account the cohesion between small particles. A comprehensive analysis of formula (2) for critical threshold velocity that accounts for the variability of the coefficient A was conducted by Li et al. (2014).

For any particular sand bed there exists a threshold value of shear velocity beyond which grain detachment begins. This critical velocity is known as the fluid threshold. The shear stress τ is proportional to the velocity gradient and equal to $\mu\frac{\partial u}{\partial y}\big|_{y=0}$, where μ is the local dynamic viscosity of the fluid, u is the fluid velocity which is parallel to the surface and y is the axis locally normal to the surface with its origin at the surface. The goal of this work is to study the wind flow in a wind tunnel over ripples bedform using the commercial CFD (Computational Fluid Dynamics) software ANSYS Fluent. Whereas few such studies of flows over dunes topography have been conducted in the past (Parsons et al., 2004; Herrmann et al., 2005; Schatz and Herrmann, 2006) and their potential for dune research have been discussed (Livingstone et al., 2007), to the best of our knowledge none has been done for sand ripples.

Wind tunnel experiments are one of the common methods to study the evolution of ripples and their characteristics (see review in Rasmussen et al. (2015)), but the details of the wind flow over the ripples are still unexplored. In the present study we address this issue by using two-dimensional simulations of the flow without sand flux in the wind tunnel of the Aeolian Simulation Laboratory of the Ben-Gurion University. Despite the fact that in most aeolian situations the air flow will interact with the sand flux (see Kok et al. (2012)), our results will help to understand the pattern of the flow over the ripples and the initial response of the bedform to different wind velocities.

The stationary wind tunnel in the Aeolian Simulation Laboratory in the Ben-Gurion University (BGU) is described in Pye and Tsoar (2009) and Katra et al. (2014). The BGU wind tunnel is an open circuit wind tunnel composed of three sections: an entrance cone, a test section and a diffuser (see Fig. 1). The tunnel is configured for air suction mode whereby air is fed into the tunnel through the bell-shaped entrance by a fan located at the end of the diffuser. The maximum air flow speed measured at the central section of a tunnel at a distance of 0.15 m from the inlet is 25 m/s. The cross sectional area of a tunnel is 0.7×0.7 m² and the working length is 12 m (7 m of test section) test section. Insets A and B in Fig. 1 show different overall views of the wind tunnel and arrow indicates the flow direction. The wind tunnel has a feeder (seen at the upper left corner of inset B) for controlling the saltation flux

in the test section. This is a medium wind tunnel according to the classification of Rasmussen et al. (2015).

2. Numerical model

For this numerical study we use ANSYS Fluent (see ANSYS Manual, http://www.ansys.com/Support/Documentation). The details of the implementation of the numerical code are elaborated in the following subsections.

2.1. Geometry and meshing

We considered a two-dimensional (2D) rectangular control volume whose height corresponds to the wind tunnel experiment and equals 0.7 m. The width of the control volume (i.e. the length in the dimension parallel to the shearing flow) of 1.063 m was chosen such that it is short enough to be numerically efficient with reasonably fine mesh while long enough to ensure that the mean flow and the small-scale flow features in the vicinity of the ripples do not change appreciably along the direction of the flow. The upper boundary of the control volume is a non-moving smooth wall, while the bottom is a non-moving wavy wall shaped by a periodic pattern of ripples. The basic form of a ripple is asymmetric and shown in Fig. 2a and b and its shape was taken from a previous wind tunnel study (Schmerler et al., 2015, see Table 1 which summarizes the ripples morphology in the experiments). The inlet boundary condition is posed at the left boundary of the control volume while the outlet boundary condition is posed at the right boundary of the control volume.

In constructing the mesh we used an adaptive mesh which is refined in the vicinity of the wavy wall in order to capture fine features of the flow (see Fig. 2c). General view of the control volume geometry and the mesh are shown in Fig. 3.

2.2. Setup and solution

We use a steady-state density-based 2-D solver. The operating conditions are pressure of 1 atm and a temperature of 300 K at
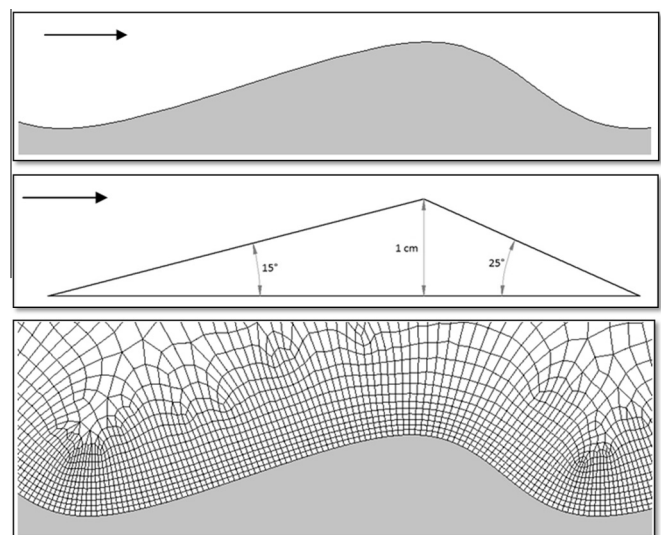

Fig. 2. (a) Ripple profile. The shape of the ripple was approximated by splines passing through the measured topography of the ripples formed in the wind tunnel. The arrow in the top left indicates the direction of the shearing mean flow. The skeleton and scaling are given in Fig. 2b. (b) Skeleton of a ripple is based on measured topography of the ripples formed in the wind tunnel. The arrow in the top left indicates the direction of the shearing mean flow. The length of the bottom edge is fully determined by the rest of the parameters and it is approximately 5.877 cm.

Fig. 1. Wind tunnel of the Aeolian Simulation Laboratory (Ben-Gurion University of the Negev) with sand bed covered by ripples.

Table 1
Morphometric characteristics of ripples for different sand size fractions in wind tunnel experiments (Schmerler et al., 2015). Values in the parentheses show standard deviation.

| u_* (m/s)	Wavelength (mm)	Height (mm)	Ripple index
Grain size: 247–300 μm			
0.37	72.45 (15.0)	3.01 (0.39)	24.29 (2.40)
0.47	74.62 (3.88)	2.85 (0.24)	26.35 (1.71)
0.63	105.23 (6.49)	4.12 (0.30)	25.66 (2.08)
0.77	166.04 (15.77)	5.92 (0.37)	28.13 (3.26)
0.98	248.14 (31.02)	8.14 (1.70)	31.79 (7.87)
Grain size: 200–247 μm			
0.34	74.69 (5.70)	2.80 (0.43)	27.01 (2.02)
0.42	78.43 (4.16)	2.88 (0.35)	27.63 (3.34)
0.59	101.12 (9.20)	3.88 (0.39)	26.20 (2.57)
0.72	139.54 (9.84)	5.97 (0.30)	23.37 (1.23)
0.98	200.87 (9.80)	8.24 (0.58)	24.53 (2.37)
Grain size:142–200 μm			
0.32	80.73 (5.76)	3.00 (0.31)	27.19 (3.27)
0.47	95.83 (5.14)	4.24 (0.30)	22.71 (1.78)
0.63	112.84 (7.59)	6.18 (0.67)	18.39 (1.28)
0.75	151.82 (7.79)	7.36 (0.67)	20.74 (1.61)
0.93	217.65 (24.45)	8.83 (1.11)	24.79 (2.42)
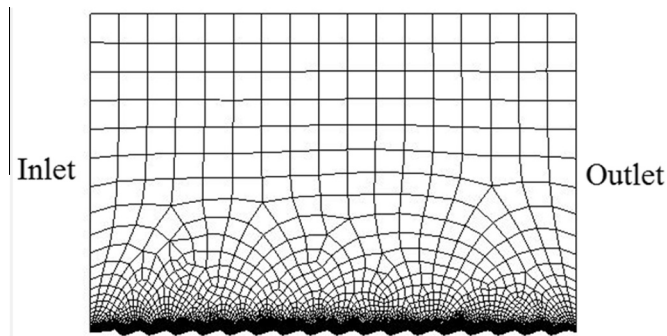
Fig. 3. Control volume and mesh. Mesh is refined in the vicinity of the bottom wall to capture fine-scale flow structures.

the inlet and outlet. At the upper and bottom boundaries of the computational domain we pose no-slip solid wall boundary conditions for velocity and zero heat flux (thermally isolated wall) for temperature. At the inlet we defined a uniform normal-to-plane flow with turbulent intensity of 10% and turbulent length scale of 5 cm which were selected based on geometry, inlet velocity and general characteristics of atmospheric turbulent flows. The obtained results are not very sensitive to the magnitude of these parameters. In the outlet an outlet-vent boundary condition was chosen with constant atmospheric pressure. In simulations we employed the popular SST (shear stress transport) k-omega turbulence model (see e.g. Menter (1994)) since the main goal of this study is to determine shear stress distribution at the wall. We have also found that under the change of the turbulence model to another popular k-epsilon model, the main parameters of the flow (the shape of separation bubble, the length required for attaining fully developed flow and mean velocity distribution) do not vary appreciably. As in all turbulence models, SST model has a number of parameters which must be specified. In the calculations we used the default values of these parameters in ANSYS Fluent. In order to ensure full convergence for the density-based solver, we used the solution steering option that is a solver convergence tool in ANSYS Fluent for density-based steady-state solutions. The blending parameter in the steering option determines the ratio of the second-order blending accuracy to the first-order accuracy of the discretization schemes. In the simulations we used a varying

blending parameter depending on the ripple height, typically 50–75%. The rest of the parameters used with the steering option were the default values. In the calculations we used the equation of ideal gas as equation of state of air. The density-based solver solves the energy conservation equation together with momentum and mass conservation equations. It should be emphasized that we considered a single phase flow over a rough surface with no regard to the influence of the saltating sand grains as was done for barchan dunes by Herrmann et al. (2005) and transverse dunes by Schatz and Herrmann (2006).

2.3. Code validation

We verified the compliance of the calculated velocity fields with the non-slip solid wall boundary conditions and mass conservation between the inlet and the outlet. Another test was made by increasing the height of the control volume by a factor of 2 to make sure that the flow near the ripples is not affected by the location of the upper wall. The mesh was validated by increasing mesh density to make sure that the selected mesh is not too rough to miss fine features of the flow. We have also verified that the mesh is dense enough to resolve the structure of the boundary layer. To this end the distance of the nearest point in the mesh to the sand bed y must satisfy the condition, $y^+ = yu_*/v < 10$ (for details see Landau and Lifshitz, 1999, p. 175, Fig. 31) where v is the fluid kinematic viscosity ($2 \cdot 10^{-5}$ m²/s for air).

3. Numerical results and discussion

For a typical inlet velocity of $u_\infty = 7$ m/s and ripple height of the order of 1 cm, the mean flow field develops quickly. The interesting fine features of the flow are the vortices between the neighboring ripples (see Figs. 4 and 5). Clearly, the emergence of the vortices depends on the geometry of the ripples and incoming flow velocity and fluid parameters. In the case where vortices are not formed the flow velocity is in the direction of the shearing flow. The flows with vortices are similar to those observed in flows over a cavity or like the separation bubble over barchan dunes (Herrmann et al., 2005). Evidences for the existence of such vortices above ripples were found in wind tunnel experiments by Tong and Huang (2012).

At the initial stage of saltation sand grains are detached from the sand bed due to shear stress produced by the flow and at later stage the impact mechanism becomes the dominant mechanism for sand transport (Kok et al., 2012). Consequently, we calculated the shear stress distribution at the bottom wall of the tunnel covered with sand ripples. The shear stress was recorded using a built-in option in the ANSYS Fluent code. We repeated simulations for different inlet velocities $u_\infty = 5$ m/s, 7 m/s, 9 m/s and for different ripple heights. In these calculations we changed only the height of the middle point in the ripple skeleton h (e.g. $h = 1$ cm in Fig. 2b). Calculations were performed for $h = (0.25, 0.5, 0.75, 1.0, 1.333, 1.667, 2, 2.5)$ cm. It must be noted that in the wind tunnel experiments ripples were flattened for inlet velocity $u_\infty \geqslant 12.5$ m/s for 200–247 μm sand fraction. In addition, in all the wind tunnel experiments the height of the formed ripples was $h \leqslant 2$ cm (Schmerler et al., 2015).

We selected a ripple located at $x = 0.8$ m, where the x-axis is defined as the distance from the inlet. This location is chosen for being at an appropriate distance from the inlet to ensure fully developed flow and an appropriate distance from the outlet to ensure that the backflow or gauge pressure effects do not affect the flow appreciably. At this ripple we recorded the maximum shear stress (one of ANSYS Fluent possible outputs) which is always attained in the vicinity of the crest of the ripple. In addition, we recorded the minimum shear stress in the trough between two
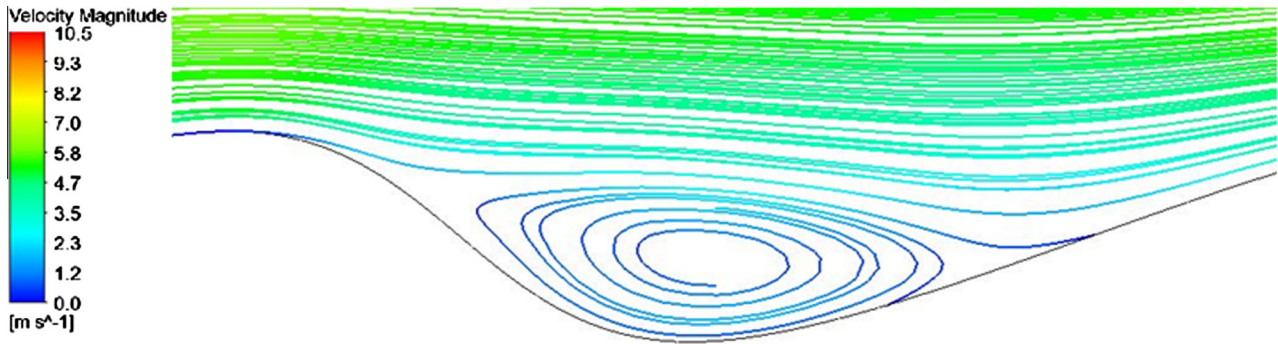
Fig. 4. Streamlines of the flow inside the trough between two ripples with height of $h = 1$ cm and wind velocity of $u_\infty = 7$ m/s from left to right.
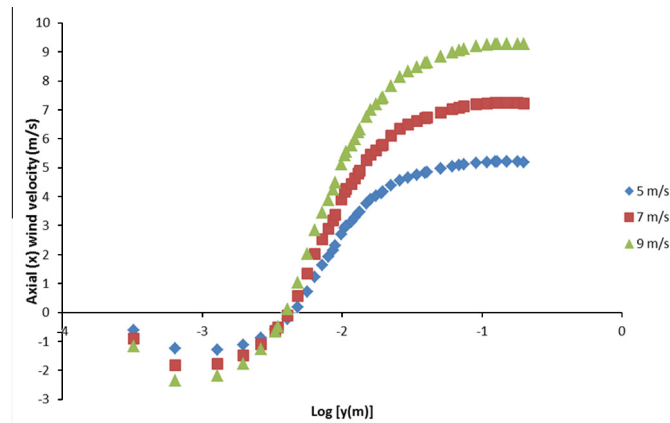

Fig. 5. Wind velocity in the axial direction (i.e. parallel to the shearing flow) inside the trough between two ripples with height of $h = 1$ cm at $x = 0.775$ m for different wind velocities. The x-axis is the logarithm of the vertical height from the bottom of the trough.

successive crests. It should be noted here that when there are vortices between ripples, as occurs in most of the simulations, the minimum shear stress is negative, i.e. with direction opposite to the mean flow direction. In the case of high ripples we observed two minima of shear stress between each two ripples and recorded the global minimum. When the height of the ripple is small, $h = 0.25$ cm, and for and vortices are not formed and the minimum shear stress is positive. In Fig. 6 we presented shear stress profile over sand ripples.

Fig. 7 shows the ratio of maximum to minimum absolute values of shear stresses at the ripple surface as a function of the inlet wind velocity (5, 7 and 9 m/s). Clearly, this ratio equals 1 for a smooth surface (i.e. without ripples). The ratio reaches an approximately

constant value of 2.5—2.9 for all inlet wind velocities from a ripple height of about 1 cm as the maximum and the minimum shear stress increase with the ripple height as shown in Fig. 8.

Fig. 8 shows the maximum and the minimum shear velocities at the ripple crests and troughs for different ripple heights and wind velocities. The shear velocity at the crest grows for ripple height below 1 cm and changes very little for ripples higher than 1 cm. For inlet wind velocity of 9 m/s a pretty high shear velocity of $u_* = 0.6$ m/s was recorded in the simulations. Note that sharp decrease of shear velocity obtained for the smallest ripple height is associated with the absence of vortex under these conditions. Otherwise, inspection of Fig. 8 reveals that all curves have a similar shape.

The maximum shear velocity as a function of inlet wind velocity for different ripple heights is shown in Fig. 9. This figure demonstrates a near-perfect linear dependence of the maximum shear velocity at the sand bed on the inlet wind velocity, for all ripple heights.

Experimental observations in the wind tunnel (Schmerler et al., 2015) show that: (i) for inlet velocity $u_\infty = 12.5$ m/s and for sand grains size 200–247 μm ripples are destroyed; (ii) ripples having a height $h > 2$ cm are not formed even for 300–347 μm sand grains (see Table 1). The calculated shear velocity according to Eq. (1) as a function of grain diameter is shown in Fig. 10. It is clear that for 300 μm grains $u_{*t} \approx 0.3$ m/s, while for 7 m/s inlet speed the shear velocity at the crest exceeds 0.3 m/s even for small ripples having a height of 0.25 cm (see Fig. 8). This 7 m/s inlet speed stands in contrast to the wind tunnel experiments where ripples are destroyed only at 12.5 m/s wind speed. The question then arises why ripples exist in the wind tunnel for shear velocities higher than the calculated fluid threshold? The answer is related to the effect of the saltation layer which is defined as the height below which 50% of the mass flux is attained (Kok et al., 2012) and its height is about 2–3 cm above the sand bed.
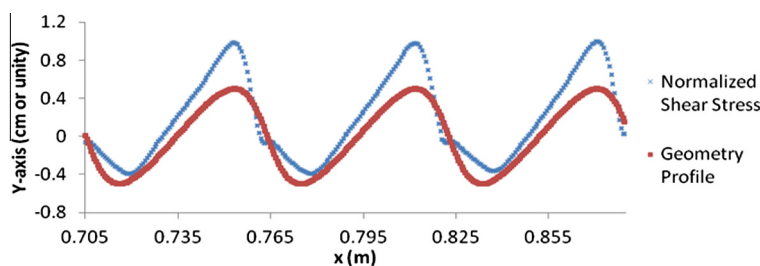

Fig. 6. Shear stress distribution at sand ripples surface with height of $h = 1$ cm and wind velocity of $u_\infty = 7$ m/s. The shearing flow direction is from left to right. The red rectangles represent the ripples profile and the blue crosses represent the normalized shear stress, τ/τ_{max}, using the maximum shear stress in the segment taken. The x-axis coordinate is the distance along the control volume with origin at the inlet. The y-axis is shared for both curves but should be interpreted as cm for ripple geometry and unity for the normalized shear stress (which is 1 at the crest).
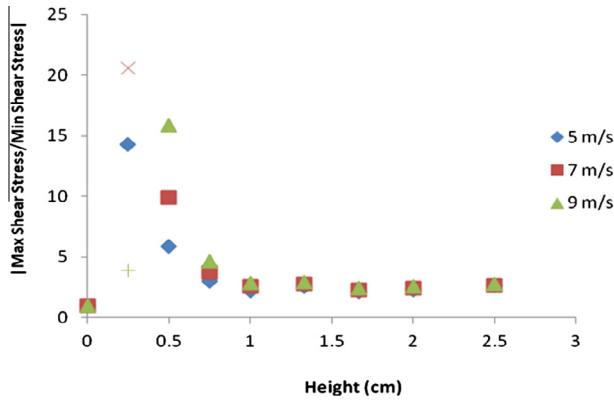
Fig. 7. Ratio of maximum to minimum absolute values of shear stresses at the ripple as a function of ripple height for several inlet velocities. Notice that at a height of 0.25 cm there are two cases in which a vortex is not formed: for m/s (indicated by ×) and m/s (indicated by +). Obviously at the limit of height → 0 the ratio approaches unity.
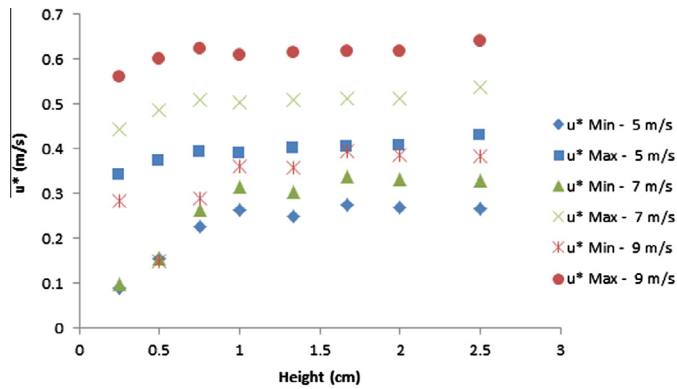

Fig. 8. Shear velocity at the sand ripples surface as a function of ripple height for three different inlet wind velocities. For each wind velocity two sets are plotted, the maximum shear velocity and the minimum.

Indeed, our numerical analysis does not include the effect of saltating particles that is very important for ripple formation. It was shown using adequate physical saltation models that shear velocity is reduced in the presence of saltation (see Fig. 13 in Kok et al., 2012; Bauer, 2013). These numerical results contradict Owen's hypothesis that the surface shear velocity remains at the impact threshold which is roughly 0.8 times the fluid threshold velocity (Owen, 1964). It is conceivable to suggest that fluid shear
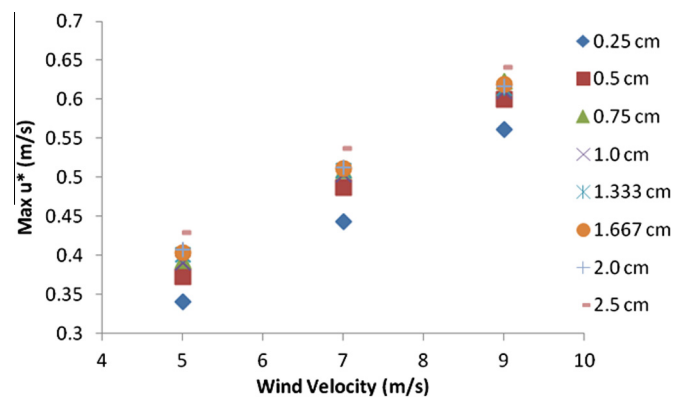

Fig. 9. Maximum shear velocity at the sand ripples surface as a function of the inlet wind velocity for all ripple heights tested.
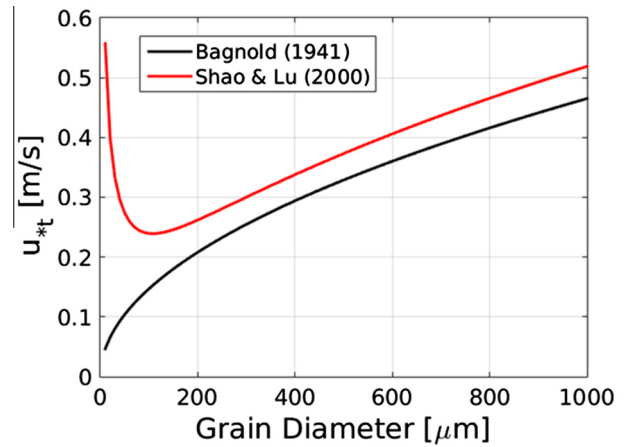

Fig. 10. Fluid threshold velocity as a function of grain diameter according to Bagnold (1941) and Shao and Lu (2000). Note that Shao and Lu (2000) take into account the effect of cohesion between the particles which leads to the minimum in the curve.

stress is reduced in the presence of saltation layer because a fraction of the total shear stress in particle-air suspension is borne by the saltating grains. Consequently, the fluid shear velocity estimated from the wind speed measurements inside the saltation layer should yield smaller values than those measured above the non-erodible bed. The effect of the saltation layer is due to the dominance of splash entertainment mechanism in steady state saltation (Kok et al., 2012).

Therefore, without effect of saltation only small ripples would be formed, namely those where shear velocity at the surface is below the impact threshold. The condition for ripple flattening by fluid flow shear is $u_{*,tr} > u_{*t}$, where $u_{*,tr}$ is shear velocity at the trough, and for $u_{*,cr} > u_{*t}$, where $u_{*,cr}$ is shear velocity at the crest. Under these conditions the crest will be eroded and this is the mechanism which limits ripple growth. Similar mechanism was suggested for megaripples by Katra et al. (2014) and Yizahq and Katra (2015).

The simulated shear stress distribution over the sand ripples is important at the initial phase of saltation before the development of steady state saltation where the effect of saltation layer is small. At this transient stage sand grains from the crests will be dislodged as the shear stress at the surface is larger than the fluid threshold.

The separation bubble found in the simulations, which is new in the context of ripples, may play a role in determining the ripple wavelength as in this region the sand flux will be smaller than the flux at the wind slope. Therefore, effectively the separation bubble acts as a shadow zone in Sharp theory (1963). Further studies are required in order to investigate the sizes of the separation bubble including wind tunnel experiments designed to validate its existence and its effect on ripple morphology.

4. Summary and conclusions

The wind flow over 2D sand ripples in wind tunnel has been studied using ANSYS Fluent simulations for different inlet velocities and ripples heights. Simulations show that shear stress at the crest is about 2.5 times larger than the shear stress at the trough and that in most of the simulations a separation bubble has been formed at the lee slope. These results highlight the importance of the effect of the saltation on the shear stress at the surface since without saltation only small ripples will be formed. Ripples will exist as long as the shear velocity at the surface will be below the impact threshold for the specific grain size. Extension of the

simulations to three-dimensional ripples with different curvature segments will help to understand stability of normal ripples to transverse perturbations (Yizhaq et al., 2012).

Acknowledgments

References

Anderson, R.S., 1987. A theoretical model for aeolian impact ripples. Sedimentology 34, 943–945.

Anderson, R.S., Bunas, K.L., 1993. Grain size segregation and stratigraphy in aeolian ripples modelled with a cellular automaton. Nature 365 (6448), 740–743.

Bagnold, R.A., 1941. The Physics of Blown Sand and Desert Dunes. Dover Publications Inc, Mineola, New York.

Durán, O., Claudin, P., Andreotti, B., 2014. Direct numerical simulations of aeolian sand ripples. PNAS 111 (44), 15665–15668.

Bauer, B.O., 2013. Fundamentals of aeolian sediment transport: boundary-layer processes. In: Treatise on Geomorphology. In: Shroder, J., Lancaster, N., Sherman, D.J., Baas, A.C.W. (Eds.), . Aeolian Geomorphology, vol. 11. Academic Press, San Diego, CA, pp. 7–22.

Herrmann, H.J., Andrade, J.S., Schatz, V., Sauermann, G., Parteli, E.J.R., 2005. Calculation of the separation streamlines of barchans and transverse dunes. Phys. A 357, 44–49.

Katra, I., Yizhaq, H., Kok, J.F., 2014. Mechanisms limiting the growth of aeolian megaripples. Geophys. Res. Lett. 41, 858–865.

Livingstone, I., Wiggs, G.F.S., Weaver, C.M., 2007. Geomorphology of desert sand dunes: a review of recent progress. Earth Sci. Rev. 80, 239–257.

Owen, P.R., 1964. Saltation of uniform grains in air. J. Fluid Mech. 20 (225–242), 19.

Kok, J.F., 2008. Electrostatics in wind-blown sand. Phys. Rev. Lett. 100, 014501, 1–4.

Kok, J.F., Parteli, E.J.R., Michaels, T., Karam, D.B., 2012. The physics of wind-blown sand and dust. Rep. Prog. Phys. 75, 106901.

Landau, L.D., Lifshitz, E.M., 1999. Fluid Mechanics. Butterworth-Heinemann, Oxford.

Li, B., Ellis, J.T., Sherman, D.J., 2014. Estimating the impact threshold for wind-blown sand. J. Coastal Res. 70 (sp1), 627–632.

Manukyan, E., Prigozhin, L., 2009. Formation of aeolian ripples and sand sorting. Phys. Rev. E 79, 031303, 1–10.

Menter, F.R., 1994. Two-equation eddy-viscosity turbulence models for engineering applications. AIAA J. 32, 1598–1605.

Parsons, D.R., Walker, I.J., Wiggs, G.F.S., 2004. Numerical modeling of flow structures over idealized transverse aeolian dunes of varying geometry. Geomorphology 59, 149–164.

Prigozhin, L., 1999. Nonlinear dynamics of aeolian sand ripples. Phys. Rev. E 60, 729–733.

Pye, K., Tsoar, H., 2009. Aeolian Sand and Sand Dunes. Springer-Verlag, Berlin Heidelberg.

Rasmussen, K.R., Valance, A., Merrison, J., 2015. Laboratory studies of aeolian sediment transport processes on planetary surfaces. Geomorphology 244, 74–94.

Schatz, A., Herrmann, H.J., 2006. Flow separation in the lee side of transverse dunes: a numerical investigation. Geomorphology 81, 207–216.

Shao, Y., Lu, H., 2000. A simple expression for wind erosion threshold friction velocity. Geophys. Res. J. 105, 22437–22443.

Sharp, R.P., 1963. Wind ripples. J. Geol. 71, 617–636.

Schmerler, E., Katra, E., Kok, J.F., Tsoar, H., Yizhaq, H., 2015. Experimental and numerical study of Sharp's shadow zone hypothesis on sand ripple wavelength. Submitted to Aeolian Research.

Tong, D., Huang, N., 2012. Numerical simulation of saltating particles in atmospheric boundary layer over flat bed and sand ripples. J. Geophys. Res.: Atmos., 1984–2012

Wiggs, G.F.S., 1997. Sediment mobilization by the wind. In: Thomas, D.S.G. (Ed.), Arid Zone Geomorphology. John Wiley, New York, pp. 351–372.

Yizhaq, H., Balmforth, N.J., Provenzale, A., 2004. Blown by wind: nonlinear dynamics of aeolian sand ripples. Physica D 195, 207–228.

Yizhaq, H., Katra, I., Kok, J., Isenberg, O., 2012. Transverse instability of megaripples. Geology 40, 459–462.

Yizhaq, H., Katra, I., 2015. Longevity of aeolian megaripples. Earth Planet. Sci. Lett. 422, 28–32.